Energy 171 (2019) 385–392

Contents lists available at ScienceDirect

Energy

journal homepage: www.elsevier.com/locate/energy

The role of air density in wind energy assessment – A case study from Germany

Christopher Jung*, Dirk Schindler

Environmental Meteorology, Albert-Ludwigs-University of Freiburg, Werthmannstrasse 10, D-79085 Freiburg, Germany

ARTICLE INFO

Article history:
Received 13 November 2018
Received in revised form
18 December 2018
Accepted 9 January 2019
Available online 11 January 2019

Keywords:
Air density
Wakeby distribution
WSWS
Power curve
Wind turbines
Germany

ABSTRACT

The statistical air density distribution was modeled on a high-spatial resolution scale (200 m × 200 m) and the error by using constant standard air density was estimated using Germany as study area. Daily mean air temperature and air pressure time series of 144 meteorological measuring stations operated in the period 1979–2014 were used to calculate air density in the very common hub height for newly installed wind turbines of 140 m. The parameters of the statistical air density distributions were mapped for the whole of Germany. By applying a 2.4 MW power curve and the wind speed-wind shear model, study area-wide annual energy yield was calculated assuming constant standard air density and using the modeled air density distributions. The results from the comparison of the energy yields demonstrate that the total area with energy yield >7.0 GWh/yr is slightly smaller (0.7%) when air density is considered to be variable. Based on the results of this study, the influence of air density on the wind energy yield of low elevation coastal sites and high elevation mountain sites can now be quantified in the study area. This will contribute to a more efficient use of the wind resource.

1. Introduction

Wind energy is an energy source that can make a substantial contribution to reducing greenhouse gas emissions and has the potential to cover a large amount of global electricity demand [1]. To meet the current global electricity demand, a cumulative installed wind capacity of about 10,800,000 MW is necessary [2]. By the end of 2017, the installed wind capacity was 539,581 MW [3] which means that many new wind turbines more will have to be installed for covering the global electricity demand. However, in many countries, suitable sites for new wind turbine installations are rare [2]. On the one hand, this is due to the fact that geographical restrictions such as urban areas, permafrost areas, and conservation areas limit the available area [2]. On the other hand, the productive wind resource and the corresponding wind turbine power output (P_w) are also limited. In general, P_w can be described by:

$$P_W = \frac{1}{2}\rho A U^3 C_P \quad (1)$$

with ρ the air density in wind turbine hub height (h_{hub}), A being the rotor swept area, U is the wind speed in h_{hub} and C_p is the Betz's power coefficient [4]. Both A and C_p are features of wind turbines whereas U and ρ are properties of the wind turbine environment. Since P_w changes with the cube of U, the spatio-temporal variability of U has a much greater influence on P_w than ρ [5]. Thus, many recent studies aim to improve the spatio-temporal description of U and other very closely related wind variables.

At a site near Lake Erie (Ohio, USA), wind energy potential was assessed by U, turbulence intensity, distributional parameters of U, wind direction, wind power density, and wind turbine capacity factors [6]. Germany's directional P_W was calculated by using the mixed Burr-Generalized Extreme Value distribution and Gaussian copulas for establishing a functional relationship between U and wind direction [7]. The suitability for installing wind turbines at two sites in Chile was evaluated by using U data from the numerical Weather Research and Forecasting (WRF) model [8]. In another study, wind power density in hub height was mapped in Iran based on U data from 150 measurement stations [9]. The wind resource characteristics in a complex mountain region were investigated in Chenzhou (China) [10]. Considering the great three-dimensional spatial variability of U, the wind speed-wind shear model (WSWS) was parameterized at a 200 m × 200 m horizontal resolution in the entire wind turbine hub height range in Germany [11]. The inter-annual variability of the wind resource was quantified by

* Corresponding author.
E-mail address: christopher.jung@mail.unr.uni-freiburg.de (C. Jung).

https://doi.org/10.1016/j.energy.2019.01.041
0360-5442/

Abbreviations

Acronyms

asl	above sea level
GEV	Generalized Extreme Value distribution
MLR	multiple linear regression model
WRF	Weather Research and Forecasting model
WSWS	wind speed-wind shear model

Symbols

$\widetilde{R^2}$	median coefficient of determination
R^2	coefficient of determination
$\overline{T}_a$	mean air temperature (°C)
T_a	air temperature (°C)
C_P	Betz's power coefficient
$\widehat{F}_i$	estimated cumulative probability of the ith empirical value
$\overline{F}$	mean of the empirical cumulative distribution function values
F_i	ith empirical cumulative distribution function value
p	air pressure (hPa)
$\overline{p}$	mean air pressure (hPa)
$\overline{\rho}$	mean air density (kg/m^3)
$\tilde{\rho}$	median air density (kg/m^3)
ρ_{st}	standard air density (1.225 kg/m^3)
ρ	air density (kg/m^3)
$\Delta\rho$	air density difference (kg/m^3)
A	rotor swept area (m^2)
AEY	air density corrected mean annual energy yield (GWh/yr)
AEY_{st}	mean annual energy yield assuming standard air density (GWh/yr)
APE	absolute percentage error (%)
b	regression parameter
c	constant
el	elevation (m asl)
f	probability density function
F^{-1}	quantile function
G	atmospheric gas constant for dry air (287.058 J/kgK)
h_0	ground level height (m)
h_{hub}	wind turbine hub height (m)
lat	latitude (°)
lon	longitude (°)
PE	percentage error (%)
P_w	wind turbine power output (kW)
RE	relative error (GWh/yr)
U	wind speed (m/s)
U_{st}	wind speed of standard power curve (m/s)
z	air density correction
δ	second Wakeby shape parameter
α	first Wakeby scale parameter
β	first Wakeby shape parameter
γ	second Wakeby scale parameter
ε	Wakeby location parameter

performing an annual parameterization of WSWS [12].

Substantially fewer research was carried out focusing on ρ and its influence on P_W. A multivariate wind distribution model including U, wind direction, and ρ was developed for one onshore and one offshore location in the USA [13]. A bivariate probability model was presented for the Canary Islands (Spain) taking the variability of ρ and U into account [14]. In the same study area, Díaz et al. [15] compared eight measure-correlate-predict-models to simulate the wind power density. They included ρ in the model parameterization and concluded that it is important to consider the annual variation of ρ even in regions at the sea level. The uniform distribution was used for a case study in the southern Caspian Sea to describe the air density distribution [16]. The sensitivity of P_W to ρ was evaluated for a wind farm in Spain. It was found that, when ρ is varied from −5% to +5%, P_W error lies between −2.40% and +2.22% [17]. To minimize the errors resulting from ignoring the spatio-temporal variability of ρ, some investigations consider the variability of ρ. For P_W assessment in Kiribati, mean ρ ($\overline{\rho}$) was calculated using air temperature (T_a) and air pressure (p) [18]. For wind resource assessment in northern Spain, ρ was considered by using the ideal gas law and meteorological data [19].

In many other previous wind energy yield assessments, ρ was assumed to be constant over time and space being 1.225 kg/m^3. Yet, a ρ value of 1.225 kg/m^3 is only valid under standard conditions with $T_a = 15$ °C and $p = 1013$ hPa [14]. Although these standard conditions are rarely met in reality, there is often no adjustment of ρ in the estimation of P_W. In fact, ρ shows a great spatio-temporal variability which is mostly determined by p. While the spatial variability of p is mainly determined by elevation (el), meteorological conditions control the temporal variability of p. As a result, ρ shows diurnal, annual, and inter-annual variability as well as long-term trends similar to U [12].

A systematic description of the statistical ρ distribution in space makes it possible to determine its influence on P_W. Yet, the few studies currently available on this topic often relate to specific sites and therefore allow only limited insight into the role of ρ in wind energy assessment. To the best of our knowledge, a systematic quantification of the areal, ρ-dependent variability of P_W has not yet been carried out although such information is important, especially when mountainous regions are considered for the installation of new wind turbines, where the influence of air density cannot be neglected. Thus, the goal of this study was a systematic evaluation of the influence of a T_a- and p-dependent spatio-temporal variability of ρ on the wind energy yield in Germany.

2. Material and methods

2.1. Overview

The analysis of the influence of air density on wind energy yield comprises the following main steps (Fig. 1): (1) Obtaining daily mean of ground level air temperature and air pressure from 144 meteorological measurement stations distributed all over Germany, (2) extrapolation of air temperature and air pressure to wind turbine hub height of 140 m, (3) calculation of air density using the ideal gas law, (4) mapping of air density percentiles by multiple linear regression (MLR) models using the independent variables elevation, longitude (lon) and latitude (lat), (5) fitting of theoretical distributions to air density percentiles, (6) air density correction of a wind turbine-specific power curve, (7) application of the wind speed-wind shear model for calculating air density corrected mean annual energy yield (AEY). All steps involved in the data preparation and data analysis were implemented with the Matlab 2018a software.

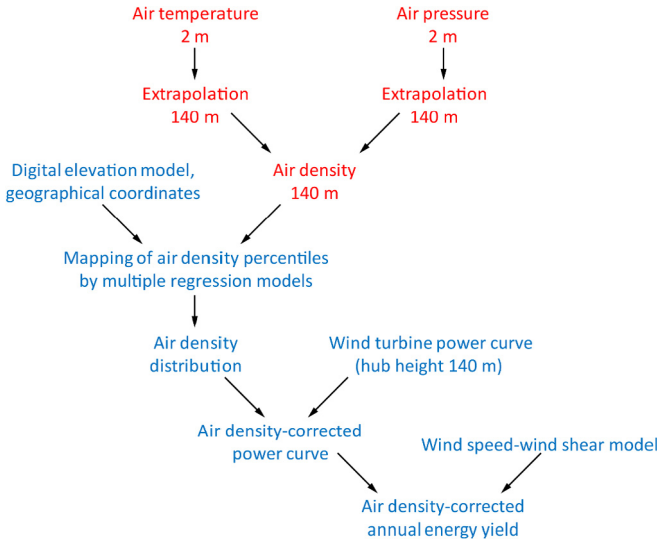

Fig. 1. Overview of the methodology applied to assess the influence of air density on wind energy yield.

2.2. Study area and data

The study area is Germany. In Germany, onshore wind energy covered in the year 2017 more than 15% of net electricity consumption. This amount of electrical energy is produced by more than 28,500 wind turbines with a total installed capacity of 50,000 MW [20]. Due to the great wind resource, the majority of the wind turbines are installed in the north of the country (Fig. 2a). Substantially fewer wind turbines are installed in the south, where the terrain is complex and the wind resource is often low.

The data used in this investigation include T_a and p time series measured at 144 meteorological measuring stations operated by the German Meteorological Service [21]. The measurement period was 1979–2014. Since T_a and p were measured at a height of $h_0 = 2$ m, they were extrapolated to h_{hub} of the wind turbine Nordex N117/2400 (140 m). The N-117 wind turbine was one of the most frequently installed wind turbine types in 2017 in Germany [18]. For the extrapolation of p to hub height, the barometric law was applied [22]:

$$p(h_{hub}) = p(h_0)\left(1 - \frac{0.0065 \cdot \Delta h}{T_a(h_0)}\right)^{5.225} \quad (2)$$

$T_a(h_{hub})$ was estimated by assuming that T_a decreases at a rate of 0.65 K/100 m [22].

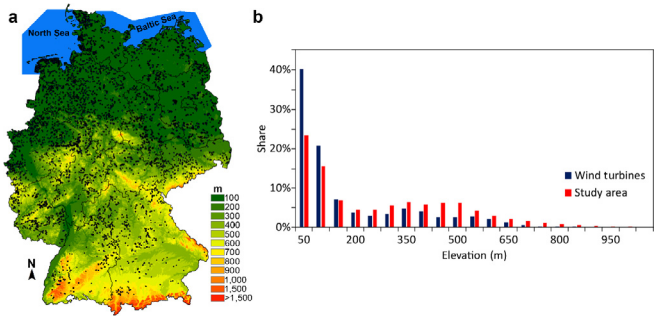

Fig. 2. (a) Study area with elevation (*el*) and existing wind turbines (black dots), and (b) share of study area and wind turbines in the study area as a function of *el*.

An overview of the measurement stations with corresponding mean T_a ($\overline{T}_a$) and mean p ($\overline{p}$) over the study period is provided in Fig. 3. In h_{hub}, low $\overline{T}_a$-values occur in southeast Germany, where the distance to the sea is greatest and *el* is often high (Fig. 3a). The lowest $\overline{T}_a$ values were measured on top of the Zugspitze ($\overline{T}_a$=−5.1 °C), which is Germany's highest mountain (*el* = 2964 m asl). Accordingly, $\overline{p}$ = 695 hPa is also very low (Fig. 3b). The warmest region in Germany is the southwest, where $\overline{T}_a$ reaches annual values up to 10.5 °C. Highest $\overline{p}$ was measured in the north of the study area because *el* is very low.

After extrapolating p and T_a to h_{hub}, ρ was calculated by the ideal gas law [2]:

$$\rho = \frac{p}{G \cdot T_a} \quad (3)$$

with G being the atmospheric gas constant (287.058 J/kgK) for dry air. In contrast to p and T_a, no simple extrapolation method for humidity to h_{hub} is available. Therefore, humidity was not considered for ρ calculation. Anyway, the resulting maximum ρ difference between dry air and saturated air is less than 1%. The resulting ρ time series were converted to empirical cumulative distribution functions.

2.3. Modeling of air density

Since *el* and the geographical location modify the meteorological conditions, both have an influence on ρ [22]. Therefore, the variables *el*, *lon* and *lat* were selected for the simulation of all percentiles of the ρ distribution with the following MLR:

$$\rho = c + b_1 \cdot el + b_2 \cdot lat + b_3 \cdot lon \quad (4)$$

where c is the constant and b_1, …, b_3 are the regression coefficients, *el* was available from a digital elevation model (resolution: 200 m × 200 m) [23].

2.4. Fitting of Wakeby distribution

To obtain continuous distributions from the modeled ρ percentiles, theoretical distributions were used. The two-parameter Gamma, two-parameter Weibull, three-parameter Burr, three-parameter Dagum, three-parameter Generalized Extreme Value (GEV), and five-parameter Wakeby distributions were fitted to the ρ empirical cumulative distribution functions by the least-squares

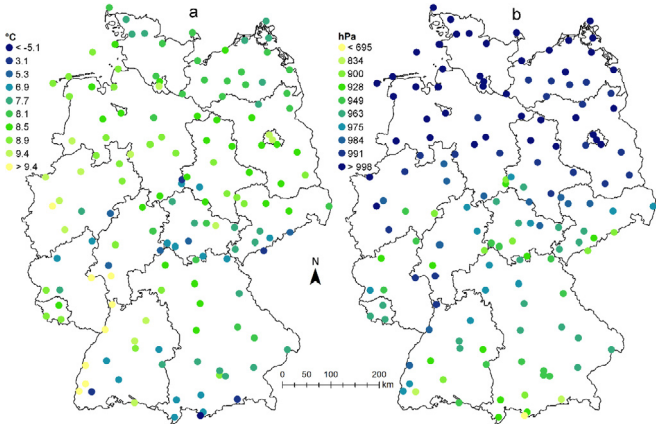

Fig. 3. Study area with (a) mean air temperature ($\overline{T}_a$) and (b) mean air pressure ($\overline{p}$) at h_{hub} = 140 m at the 144 evaluated measurement sites.

estimation method [24]. The fitting accuracy of all distributions was assessed by the coefficient of determination (R^2) which is defined as [25]:

$$R^2 = 1 - \frac{\sum_{i=1}^{n}\left(F_i - \widehat{F}_i\right)^2}{\sum_{i=1}^{n}\left(F_i - \overline{F}\right)^2} \quad (5)$$

with F_i being the ith empirical cumulative distribution function value, $\widehat{F}_i$ the estimated cumulative probability of the ith empirical cumulative distribution function value and $\overline{F}$ the mean of the empirical cumulative distribution function values. As will be demonstrated in section 3.2, the five parameter Wakeby distribution provides the highest fitting accuracy. The Wakeby distribution is typically defined by its quantile function [26]:

$$F^{-1}(\rho) = \varepsilon + \frac{\alpha}{\beta}\left[1 - (1-F)^{\beta}\right] - \frac{\gamma}{\delta}\left[1 - (1-F)^{-\delta}\right] \quad (6)$$

with α the first scale parameter, β the first shape parameter, γ the second scale parameter, δ the second shape parameter, and ε the location parameter. Its probability density function can be formulated as follows:

$$f(\rho) = \left\{\alpha[1-F(\rho)]^{\beta-1} + \gamma[1-F(\rho)]^{-\delta-1}\right\}^{-1} \quad (7)$$

2.5. Annual energy yield estimation

Wind turbine specific *AEY* for standard ρ conditions (ρ_{st}) assuming $\rho_{st} = 1.225\ \mathrm{kg/m^3}$ (AEY_{st}) is typically calculated by Ref. [2]:

$$AEY_{st} = 8,760\ hrs \int_0^{\infty} P_w(U, \rho_{st})\, f(U) dU \quad (8)$$

where $f(U)$ is the wind speed probability density and $P_W(U_{st})$ the wind turbine specific power curve.

The wind speed distributions for this study were modeled with WSWS [11,27]. WSWS enables the reconstruction of highly-resolved U [11,27] considering surface roughness and orography.

Power curves are usually available from wind turbine manufacturers. However, they are only valid for ρ_{st}. Other ρ conditions require an adjustment of the power curve. One method for wind turbine power curve adjustment was introduced by Svenningsen [28]. With this method, U of the standard power curve (U_{st}) is converted to U under real ρ conditions by:

$$U = U_{st}\left(\frac{\rho_{st}}{\rho}\right)^{z(U)} \quad (9)$$

The air density correction variable $z(U)$ is defined as:

$$z(U) = \begin{cases} \frac{1}{3} & for \quad U \le 8.0\ m/s \\ \frac{1}{3} + \frac{1}{3}\frac{U-8}{5} & for \quad 8.0\ m/s < U < 13.0\ m/s \\ \frac{2}{3} & for \quad U \ge 13.0\ m/s \end{cases} \quad (10)$$

To evaluate the effect of ρ on mean annual energy yield, AEY_{st} and *AEY* were calculated. This was done by drawing a sample of random numbers (10,000 values) from $f(U)$ and $f(\rho)$. Then, $P_W(U,\rho)$ was calculated. Finally, depending on the differences between AEY_{st} and *AEY*, the relative error (*RE*) and the absolute percentage error (*APE*) were calculated. A possible relationship between $f(U)$ and $f(\rho)$ was checked using the Pearson correlation coefficient. Since the correlation coefficient values were very low and varied in the range −0.10 to 0.10 at most measurement sites as can be seen in Fig. A1, the application of copulas did not lead to any improvement in the model, and thus, copulas were not used in *AEY* modeling.

In Fig. 4, the power curve for the applied wind turbine type [29] is presented for different ρ values (1.100 kg/m^3, 1.225 kg/m^3, and 1.300 kg/m^3). At $U < 4.0$ m/s, the influence of ρ on $P_W(U,\rho)$ is small. It is obvious that $P_W(U,\rho)$ depends most on ρ in the U range 7.0–9.5 m/s. At $U > 12.0$ m/s, when all displayed power curves operate at rated wind speed, there is no ρ-dependent difference in wind turbine power output any more. Accordingly, differences in ρ have a substantial effect (up to 15% at 7.0 m/s) on the total electricity generation in the study area if the wind speed is just below the rated wind speed at a great number of wind turbines.

3. Results and discussion

3.1. Mean air density

The parameterization of the MLR model for $\overline{\rho}$ resulted in the following equation:

$$\overline{\rho} = 1.1301 - 0.000113 \cdot el + 0.0019 \cdot lat + 0.0005 \cdot lon \quad (11)$$

The coefficient of determination ($R^2 = 0.9973$) calculated from the comparison of empirical and modeled $\overline{\rho}$ indicates a very high model accuracy. The spatial distribution of $\overline{\rho}$ is shown in Fig. 5a. It can be seen that it is mainly the influence of *el* that determines the spatial pattern of $\overline{\rho}$. In the northern parts of the study area, which are characterized by low *el* values (<100 m asl), $\overline{\rho}$ is close to ρ_{st}. In contrast, the influence of high *el* (800–1500 m asl) in the low mountain ranges in southern Germany results in very low $\overline{\rho}$ values (<1.140 kg/m^3). Values of less than $\overline{\rho} = 1.150\ \mathrm{kg/m^3}$ are not uncommon there (7% of the study area). In the German Alps, where the Zugspitze is the highest mountain, even values down to 0.900 kg/m^3 occur. In total, at 50% of the study area $\overline{\rho} < 1.205\ \mathrm{kg/m^3}$.

Fig. 5b illustrates the differences between $\overline{\rho}$ and ρ_{st} ($\Delta\rho$). It can be seen that in almost the whole of northern Germany $\overline{\rho}$ deviates only slightly from ρ_{st} ($-0.01\ \mathrm{kg/m^3} \le \Delta\rho \le 0.01\ \mathrm{kg/m^3}$). Near the

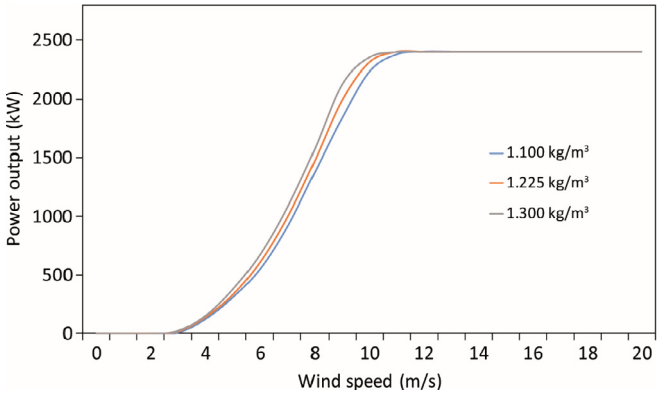

Fig. 4. Power curves for different air density (ρ) values (1.100 kg/m^3, 1.225 kg/m^3, and 1.300 kg/m^3).

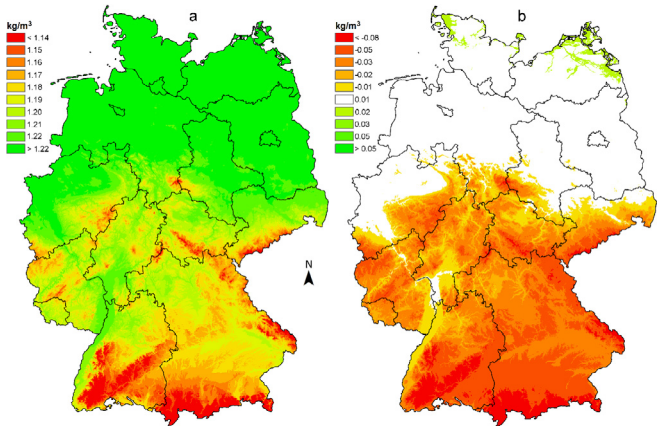

Fig. 5. (a) Mean air density ($\overline{\rho}$) and (b) air density difference ($\Delta\rho$) in the study area.

coast, there are a number of regions where $\overline{\rho}$ is higher than ρ_{st}. This is due to low *el* and low T_a. In contrast, in the middle and south of the study area there are almost exclusively regions in which $\Delta\rho < -0.01$ kg/m^3.

The results of this study demonstrate that in northern Germany, where *U* already is clearly higher than in the south [11], higher $\overline{\rho}$ is another reason why wind turbines should be installed there. In contrast, the locations suitable for using wind energy in the south are often located on exposed mountain tops where *U* is high [11], but $\overline{\rho}$ is low.

In Fig. 6, the share of $\overline{\rho}$ classes at current wind turbine locations (blue bars) is compared to the share of $\overline{\rho}$ classes found in the whole study area (red bars). Most wind turbines (26%) are located in the 1.235 kg/m^3 $\overline{\rho}$ class. These are the wind turbines close to the coast. This share of wind turbines is much higher than the share of the study area in this class (10%). In total, 49% of all wind turbines are located in regions where $\overline{\rho} > 1.225$ kg/m^3. In these areas, high *U* and high $\overline{\rho}$ both have a positive effect on *AEY*.

3.2. Probability density function of air density

In Fig. 7a, the distribution of ρ is exemplarily shown for a grid cell related to the city of Angermünde (*el* = 54 m asl) which is located close to the coast. For comparison, $f(\rho)$ from the mountain site Hohenpeißenberg (*el* = 977 m asl), which is located in the southern part of the study area, is displayed in Fig. 7b. While the mean wind speed at 10 m is similar at both sites (4.03 m/s in Angermünde and 4.24 m/s in Hohenpeißenberg), there are large differences in $f(\rho)$ due to different elevation. The ρ median ($\tilde{\rho}$) of Angermünde equals ρ_{st}. In contrast, $\tilde{\rho}$ for Hohenpeißenberg is only 1.104 kg/m^3. The other percentiles also show great differences. For example, in Angermünde the fifth ρ percentile (lower end of the distribution) is 1.179 kg/m^3. This corresponds to approximately the 98 percentile of ρ (upper end of the distribution) of Hohenpeißenberg. This means that $\rho = 1.179$ kg/m^3 in Angermünde is exceeded on 95% of all days, but in Hohenpeisenberg only on 2% of all days.

In addition to the empirical distributions, Fig. 7 also shows the fitted distributions which mostly provide a very good fit to the empirical distributions. However, the two-parameter distributions (Gamma and Weibull) cannot reproduce the shape of the distributions as good as the distributions defined by three (Burr, Dagum, and GEV) or five parameters (Wakeby).

The comparison of R^2, which is shown for all theoretical distributions in Fig. 8, allows a systematic evaluation of the goodness-of-fit. The best goodness-of-fit was achieved by the Wakeby distribution with median R^2 ($\widetilde{R^2}$) being 0.9994. GEV ($\widetilde{R^2} = 0.9993$), Dagum ($\widetilde{R^2} = 0.9988$), and Burr ($\widetilde{R^2} = 0.9978$) also provide a very high goodness-of-fit. The fitting accuracy of the two-parameter distributions Gamma ($\widetilde{R^2} = 0.9940$) and Weibull ($\widetilde{R^2} = 0.9781$) is clearly worse. Based on the results of the goodness-of-fit evaluation, the Wakeby distribution was selected for distribution fitting in the entire study area.

Before the parameters of the Wakeby distribution were estimated, the ρ percentiles at each grid cell had to be modeled. Table 1 summarizes the regression coefficients and R^2 for a selection of percentiles. For all MLR models, high R^2 values (0.9919–0.9978) were obtained which indicate a good model accuracy. This is mainly due to the strong effect of *el* on the spatial distribution of ρ.

Based on the modeled ρ percentiles, the Wakeby parameters were estimated (Fig. 9). The two parameters α and β are responsible for the low ρ values on the left-hand side of the Wakeby distribution whereas γ and δ determine the high ρ values on the right-hand side [30]. The parameters α, β, and δ change very strongly in the west-east direction (Fig. 9a,b,d). This indicates that the integration of *lat* and *lon* in MLR is important. The large-scale variability of γ and ε is clearly superimposed by *el* (Fig. 9c,e).

3.3. Influence of air density on annual energy yield estimation

From the perspective of the wind energy user, it is of particular interest whether and if so, to what extent the spatial variability of $f(\rho)$ leads to changes in *AEY*. For this reason, AEY_{st} was mapped in Fig. 10a. The corresponding areal mean AEY_{st} over the entire study area is 5.79 GWh/yr. In total, at 24.4% of the study area $AEY_{st} >$ 7.00 GWh/yr. At 1.6% of the study area $AEY_{st} > 10.00$ GWh/yr.

If ρ is considered as being dependent on *el*, *lat*, and *lon*, then the

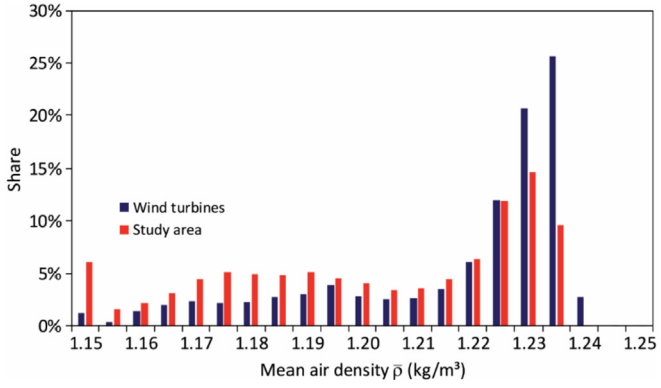

Fig. 6. Share of wind turbine locations and study area as a function of mean air density ($\overline{\rho}$) classes.

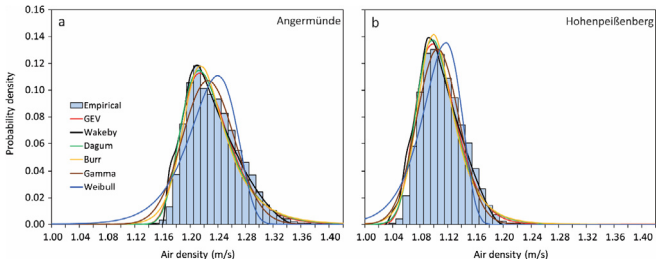

Fig. 7. Empirical probability density functions of air density (ρ) and fitted theoretical distributions ($f(\rho)$) for (a) Angermünde and (b) Hohenpeißenberg.

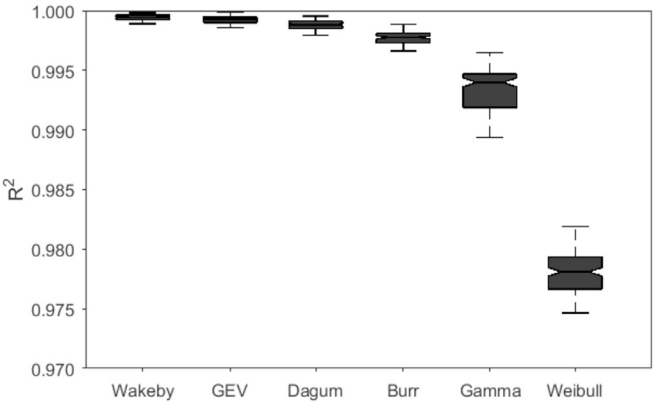

Fig. 8. Goodness-of-fit of theoretical distributions ($f(\rho)$) to empirical air density (ρ) distributions according to the coefficient of determination (R^2).

Table 1
Regression coefficients (b_1, b_2, b_3), the regression constant (c), and coefficient of determination (R^2) for MLR models associated with different air density percentiles.

Percentile	*c*	b_1	b_2	b_3	R^2
1	1.0107	−0.000100	0.0031	−0.0004	0.9942
10	1.0381	−0.000103	0.0030	−0.0004	0.9969
20	1.0614	−0.000105	0.0027	−0.0003	0.9974
30	1.0813	−0.000107	0.0025	−0.0001	0.9978
40	1.1039	−0.000109	0.0022	0.0001	0.9978
50	1.1239	−0.000111	0.0019	0.0004	0.9976
60	1.1496	−0.000114	0.0015	0.0007	0.9974
70	1.1770	−0.000117	0.0012	0.0009	0.9973
80	1.2037	−0.000120	0.0009	0.0011	0.9971
90	1.2242	−0.000125	0.0008	0.0013	0.9965
99	1.2678	−0.000134	0.0005	0.0027	0.9919

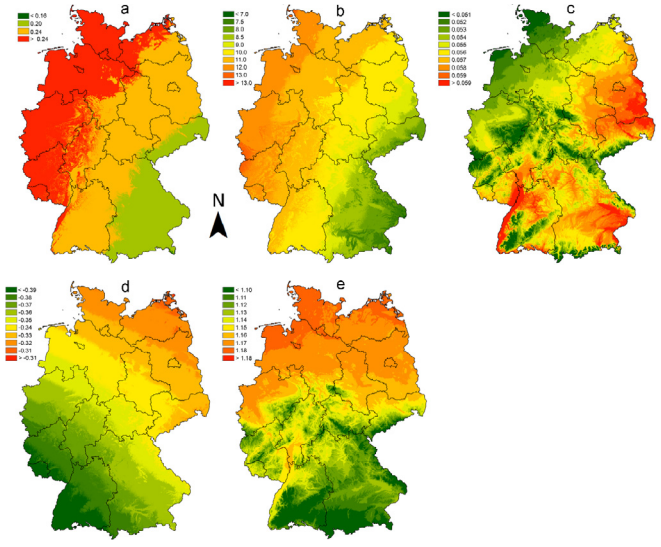

Fig. 9. Spatial distribution of the Wakeby parameters (a) α, (b) β, (c) γ, (d) δ, and (e) ε in the study area.

areal mean *AEY* will only be 5.72 GWh/yr. The area where *AEY* > 7.00 GWh/yr is then 23.7% (Fig. 10b). The size of the area where *AEY* > 10.00 GWh/yr is slightly increasing to 1.7% because of low *el* and

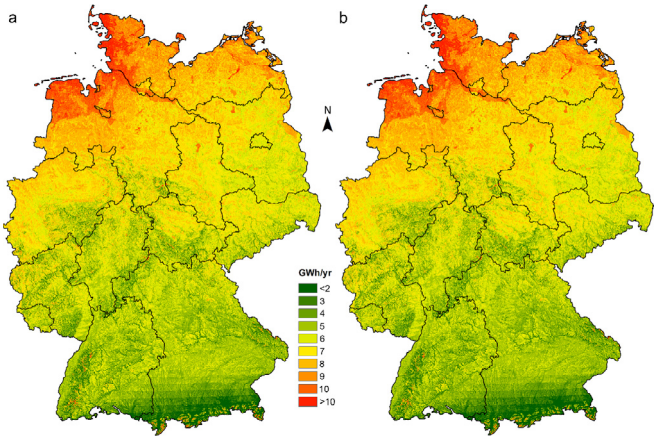

Fig. 10. (a) Mean annual wind energy yield (AEY_{st}) considering standard air density ($\rho_{st} = 1.225$ kg/m^3), (b) mean annual wind energy yield (*AEY*) considering ρ as being variable.

low T_a close to the coast.

The difference between *AEY* and AEY_{st} is shown as *RE* in Fig. 11a. Only near the coast, AEY_{st} is lower (−0.05 GWh/yr) than *AEY* (0.57% of the study area). Since the coastal regions are also regions with the high *U*, the area in which high wind energy yields can be expected is increasing. However, the areas in which the assumption of constant air density leads to higher yields than actual yields dominate. In more than 50.9% of the study area *RE* > 0.05 GWh/yr, i.e. the wind resource is overestimated. Such areas are mainly located in southern Germany where *el* is often high.

A very similar distribution of the air density-related error is reflected in *APE* (Fig. 11b). Near the coast, the wind resource is underestimated by about 0.6% due to the use of ρ_{st}. By contrast, in large parts of southern Germany, the wind resource is overestimated by up to more than 15%.

Table 2 summarizes the percentage change in *AEY* compared to AEY_{st} per 100 m increase in *el*. A total of 4.2% of Germany's surface area has *el* > 700 m. At these elevations, the influence of $f(\rho)$ causes a noticeable decrease of *AEY* by at least −5.3%. A reduction of *AEY* of more than 10% was modeled for *el* > 1300 m.

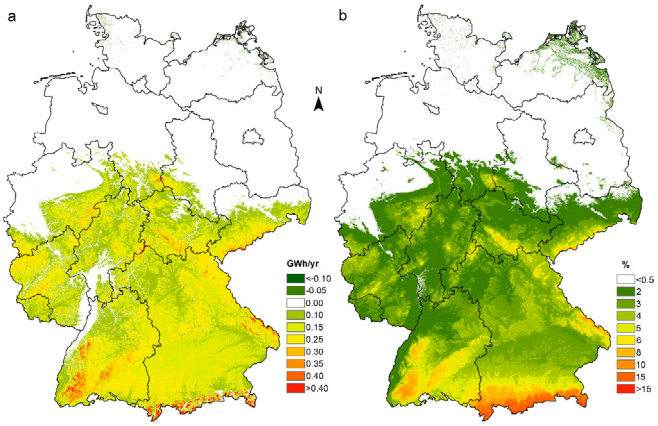

Fig. 11. Spatial distribution of (a) the relative error (*RE*), and (b) the absolute percentage error (*APE*) in the study area.

Table 2
Percentage error (*PE*) in mean annual energy yield (*AEY*) with increasing elevation (*el*).

***el* (m)**	**0**	**100**	**200**	**300**	**400**	**500**	**600**	**700**	**800**	**900**
PE (%)	0.5	−0.3	−1.1	−2.0	−2.8	−3.6	−4.4	−5.3	−6.1	−6.9
***el* (m)**	**1000**	**1100**	**1200**	**1300**	**1400**	**1500**	**1600**	**1700**	**1800**	**1900**
PE (%)	−7.8	−8.6	−9.4	−10.2	−11.1	−11.9	−12.7	−13.5	−14.4	−15.2
***el* (m)**	**2000**	**2100**	**2200**	**2300**	**2400**	**2500**	**2600**	**2700**	**2800**	**2900**
PE (%)	−16.0	−16.8	−17.7	−18.5	−19.3	−20.1	−21.8	−22.6	−23.4	−24.3

4. Conclusions

This study emphasizes the importance of considering air density in wind energy assessment, especially at high elevation. The approach and the obtained results make it possible to better compare the expected mean annual wind energy yield between candidate coastal sites at low elevation with mountain wind turbine sites at high elevation. The influence of air density on the wind energy yield of coastal and mountain sites can now be quantified on a high-spatial resolution scale. This will lead to a more efficient use of the wind resource which is due to the fact that wind turbine distribution can be optimized in the study area. The presented approach also allows an assessment of how the spatio-temporal variability of air density influences the available area of specific wind energy yield classes. As wind turbine density in Germany is already relatively high [20], possibilities are currently being sought to keep the number of new wind turbines to be installed as low as possible in order to achieve the 2030 German climate targets [20]. As most wind turbines are currently installed in the north of Germany, and the number of candidate wind turbine sites is decreasing, the pressure to install more wind turbines in the south of Germany is growing. There, most wind turbine sites are limited to elevations between 400 and 1000 m [31], where the influence of air density on the wind energy yield is already notable.

The presented modeling approach is easily portable to other regions around the world and easily allows integrating air density in wind energy assessment. In regions where air density and wind speed are strongly correlated, a further improvement of the presented modeling approach can be achieved by integrating copulas in the model development. Because information regarding variation in atmospheric stratification, which influences the rate of air temperature decrease throughout the day, were not available, daily mean air temperature and air pressure were applied instead of hourly means. If air pressure, air temperature and relative moisture is available in hub height on an hourly basis, it is recommended to extend the proposed approach to better capture the spatio-temporal variability of air density. Although the method was presented for one specific wind turbine, the calculated air density distribution can be used for any wind turbine power curve.

Conflicts of interest

This research did not receive any specific grant from funding agencies in the public, commercial or not-for-profit sectors.

Appendix

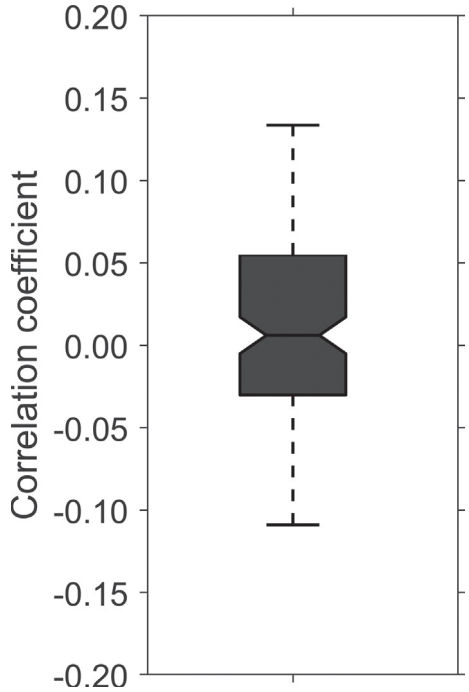

Fig. 1A. Boxplot of correlation coefficients between wind speed (U) and air density (ρ) at all measurement locations.

References

[1] Nugent D, Sovacool BK. Assessing the lifecycle greenhouse gas emissions from solar PV and wind energy: a critical meta-survey. Energy Pol 2014;65:229–44.
[2] Jung C, Schindler D, Laible J. National and global wind resource assessment under six wind turbine installation scenarios. Energy Convers Manag 2018;156:403–15.
[3] Global Wind Energy Council. Global wind statistics. 2018. accessed 01.03.18, http://gwec.net/wp-content/uploads/vip/GWEC_PRstats2017_EN-003_FINAL.pdf.
[4] Manwell JF, McGowan JG, Rogers AL. Wind energy explained: theory, design and application. second ed. Chichester: John Wiley & Sons; 2009.
[5] Shahriari M, Blumsack S. Scaling of wind energy variability over space and time. Appl Energy 2017;195:572–85.
[6] Li J, Yu XB. LiDAR technology for wind energy potential assessment: demonstration and validation at a site around Lake Erie. Energy Convers Manag 2017;144:252–61.
[7] Schindler D, Jung C. Copula-based estimation of directional wind energy yield: a case study from Germany. Energy Convers Manag 2018;169:359–70.
[8] Becerra M, Moran J, Jerez A, Cepeda F, Valenzuela M. Wind energy potential in Chile: assessment of a small scale wind farm for residential clients. Energy

Convers Manag 2017;140:71–90.
[9] Faghani GR, Ashrafi ZN, Sedaghat A. Extrapolating wind data at high altitudes with high precision methods for accurate evaluation of wind power density, case study: center of Iran. Energy Convers Manag 2018;157:317–38.
[10] Dai J, Tan Y, Yang W, Wen L, Shen X. Investigation of wind resource characteristics in mountain wind farm using multiple-unit SCADA data in Chenzhou: a case study. Energy Convers Manag 2017;148:378–93.
[11] Jung C, Schindler D. 3D statistical mapping of Germany's wind resource using WSWS. Energy Convers Manag 2018;159:96–108.
[12] Jung C, Schindler D. On the inter-annual variability of wind energy generation – a case study from Germany. Appl Energy 2018;230:845–54.
[13] Zhang J, Chowdhury S, Messac A, Castillo L. A multivariate and multimodal wind distribution model. Renew Energy 2013;51:436–47.
[14] Carta JA, Mentado D. A continuous bivariate model for wind power density and wind turbine energy output estimations. Energy Convers Manag 2007;48:420–32.
[15] Díaz S, Carta JA, Matías JM. Comparison of several measure-correlate-predict models using support vector regression techniques to estimate wind power densities. A case study. Energy Convers Manag 2017;140:334–54.
[16] Amirinia G, Kamranzad B, Mafi S. Wind and wave energy potential in southern Caspian Sea using uncertainty analysis. Energy 2017;120:332–45.
[17] Villena-Ruiz R, Ramirez FJ, Honrubia-Escribano A, Gómez-Lázaro E. A techno-economic analysis of a real wind farm repowering experience: the Malpica case. Energy Convers Manag 2018;172:182–99.
[18] Aukitino T, Khan MGM, Ahmed MR. Wind energy resource assessment for Kiribati with a comparison of different methods of determining Weibull parameters. Energy Convers Manag 2017;151:641–60.
[19] Herrero-Novoa C, Pérez IA, Sánchez ML, García MÁ, Pardo N, Fernández-Duque B. Wind speed description and power density in northern Spain. Energy 2017;138:967–76.
[20] Jung C, Schindler D. Achieving Germany's wind energy expansion target with an improved wind turbine siting approach. Energy Convers Manag 2018;173:383–98.
[21] Wetterdienst Deutscher. CDC (climate data center). 2018. accessed 02.10.18, http://www.dwd.de/EN/climate_environment/cdc/cdc_node.html;jsessionid =19E49145864F5766299478B46C1DDED1.live11042.
[22] Stull RB. Meteorology for scientists and engineers. second ed. Pacific Grove, CA: Brooks/Cole; 2000.
[23] Bundesamt für Kartographie und Geodäsie. Digitales Geländemodell Gitterweite 200 m. 2017. accessed 03.10.18, http://www.geodatenzentrum.de/geodaten/gdz_rahmen.gdz_div?gdz_spr=deu&gdz_akt_zeile=5&gdz_anz_zeile=1&gdz_unt_zeile=3&gdz_user_id=0;.
[24] Jung C, Schindler D. Global comparison of the goodness-of-fit of wind speed distributions. Energy Convers Manag 2017;133:216–34.
[25] Jung C, Schindler D, Laible J, Buchholz A. Introducing a system of wind speed distributions for modeling properties of wind speed regimes around the world. Energy Convers Manag 2017;144:181–92.
[26] Schindler D, Jung C, Buchholz A. Using highly resolved maximum gust speed as predictor for forest storm damage caused by the high-impact winter storm Lothar in Southwest Germany. Atmos Sci Lett 2016;17:462–9.
[27] Jung C, Schindler D. Development of a statistical bivariate wind speed-wind shear model (WSWS) to quantify the height-dependent wind resource. Energy Convers Manag 2017;149:303–17.
[28] Svenningsen L. Power curve air density correction and other power curve options in WindPRO. 2010. http://www.emd.dk/files/windpro/WindPRO_Power_Curve_Options.pdf.
[29] Nordex. N117/2400 (2.4 Megawatt). 2018. accessed 02.10.18, http://www.nordex-online.com/en/produkte-service/wind-turbines/n117-24-mw.html.
[30] Houghton JC. Birth of a parent: the Wakeby distribution for modeling flood flows. Water Resour Res 1978;14:1105–9.
[31] Grau L, Jung C, Schindler D. On the annual cycle of meteorological and geographical potential of wind energy: a case study from Southwest Germany. Sustainability 2017;9:1169.